AWARD NUMBER: 05HQGR0044

Recipient: University of California, Santa Barbara/Institute for Crustal Studies

Principal Investigators: Pengcheng Liu (University of California, Santa Barbara)
Stephen Hartzell (U.S. Geology Survey, Denver)

WAVEFORM INVERSION FOR 3D VELOCITY STRUCTURE AND CALCULATION OF SCENARIO EARTHQUAKE GROUND MOTIONS

Program Element III: Research on Earthquake Physics, Occurrence, and Effects

Research supported by the U.S. Geological Survey (USGS), Department of the Interior, under USGS award number 05HQGR0044. The views and conclusions contained in this document are those of the authors and should not be interpreted as necessarily representing the official policies, either expressed or implied, of the U.S. Government.

Award Number: 05HQGR0044

WAVEFORM INVERSION FOR 3D VELOCITY STRUCTURE AND CALCULATION OF SCENARIO EARTHQUAKE GROUND MOTIONS

Collaborative Research with Institute for Crustal Studies, University of California, Santa Barbara, and US Geology Survey, Denver

Pengcheng Liu
Institute for Crustal Studies, University of California, Santa Barbara, CA 93106-1100
Stephen Hartzell,
Box 25046, MS 966, U.S. Geology Survey, Denver CO 80225

Telephone Number: 805-893-8467 (Liu), 303-273-8572 (Hartzell)
Fax Number: 905-893-8649 (Liu), 303-273-8600 (Hartzell)
E-mail Address: pcliu@crustal.ucsb.edu; shartzell@usgs.gov

TECHNICAL ABSTRACT

This study focus on developing methods and procedures to obtain 3D velocity structure from the inversion of waveform data. We apply one kind of non-monotone trust-region algorithm to solve the nonlinear minimization problem, but with improvements to the search method to reduce the likelihood of falling into a local minimum in the objective function. The objective function consists of a weighted sum of the difference between the observed and synthetic first arrival times (calculated by a cross-correlation method) and the sum of the squared differences of the waveforms. By using this objective function we can easily move from a purely travel-time based measure to a full waveform-based measure.

A state-of-the-art 3D finite-difference code will be used to calculate the required Green's functions. This code written by the PI has significant computation-saving advantages (Liu and Archuleta, 1999a, 1999b, 2002). First, the code allows for two separate regions, an upper one with fine grid spacing, and a lower one with three-times the grid spacing. This feature allows for a fine grid space near the surface where shear-wave velocities are low without carrying the fine spacing to depth where it is not needed. In addition, the grid spacing can be made to grow in the horizontal and vertical directions, giving a further savings in computational effort. In this code we also improve the modeling of attenuation. The code has been fully tested and validated.

A preliminary investigation on the developed algorithms is performed by using the synthetic data generated from a simple 3D velocity structure (Figure 1). This testing indicates that the quasi-Newton trust region algorithm converges very fast if the initial model is not far away from the true model. Although the test problem is simple, it proves that the inversion algorithm can escape, at least, from shallow local minima, and move the trial model to the true solution. This testing also shows that B.F.G.S updating of the Hessian matrix performs better than the SR1 updating for the inversion of waveform data.

WAVEFORM INVERSION FOR 3D VELOCITY STRUCTURE AND CALCULATION OF SCENARIO EARTHQUAKE GROUND MOTIONS

Award Number: 05HQGR0044

Institute for Crustal Studies, University of California, Santa Barbara, CA 93106-1100
Stephen Hartzell,
Box 25046, MS 966, U.S. Geology Survey, Denver CO 80225

Telephone Number: 805-893-8467 (Liu), 303-273-8572 (Hartzell)
Fax Number: 905-893-8649 (Liu), 303-273-8600 (Hartzell)
E-mail Address: pcliu@crustal.ucsb.edu; shartzell@usgs.gov

Program Element III: Research on Earthquake Physics, Occurrence, and Effects
Keywords: Wave propagation; Strong ground motion; Source characteristics

NON-TECHNICAL ABSTRACT

The empirical relationship derived in the paper provides an efficient way for the numerical modeling community to incorporate the constant *Q* into their finite difference or finite element algorithm. The finite difference code has been used by several institutions (include USGS) to study complex wave propagation. The method and procedure developed in this project has potential to improve our understanding of 3D velocity structure that in turn can be used to predict realistic time history of ground motion from future earthquakes, a key component of the USGS Earthquake Hazards Reduction Program.

PROJECT DESCRIPTION AND RESULTS

1. **Introduction and Motivation**

Ground motions for potentially damaging earthquakes can be estimated from records of past events. However, the usefulness of this approach is limited by the available ground motion database. Often appropriate records for the magnitude of interest or the geologic setting do not exist. Scenario calculations of ground motions must be done for postulated earthquakes to augment data available. These calculations require knowledge of crustal velocity structure. In recent years experience has been gained from larger earthquakes such as Northridge and Kobe show the importance of three dimensional (3D) variations of velocity in controlling ground motion. Some of the most important of 3D effects occurr in sedimentary basins. Many at-risk urban areas are situated on deep sediment-filled basins. Several studies have demonstrated the importance of deep basin structure on strong-ground motions and observed damage patterns (e.g. Olsen and Archuleta, 1996; Iwata et al., 1996; Pitarka et al., 1996; Kawase, 1996; Hartzell et al., 1997; Wald and Graves, 1998; Graves et al., 1998). Calculation of ground motion time histories and seismic hazard assessment for urban basins requires knowledge of the 3D velocity structure of these basins.

Seismic reflection/refraction methods can be used to image sedimentary basins, however, these surveying methods are very costly. An alternative method is to utilize the waveforms of seismic ground motions that have passed through the basin. With the advent of special array deployments in urban areas by the USGS and the coming of ANSS, more and more ground motion records are being collected in urban areas of interest. This study will develop software and procedures for inverting waveform data to recover the 3D velocity structure of basins. The improved velocity structure can then be used to calculate more accurate ground motion for scenario earthquakes.

This study focuses on developing methods and procedures to obtain 3D velocity structure from the inversion of waveform data. We apply one kind of non-monotone trust-region algorithm to solve the nonlinear minimization problem, but with improvements to the search method to reduce the likelihood of falling into a local minimum in the objective function. The objective function consists of a weighted sum of the difference between the observed and synthetic first arrival times (calculated by a cross-correlation method) and the sum of the squared differences of the waveforms. By using this objective function we can easily move from a purely travel-time based measure to a full waveform-based measure.

A state-of-the-art 3D finite-difference code will be used to calculate the required Green's functions. This code written by the PI has significant computation-saving advantages (Liu and Archuleta, 1999a, 1999b, 2002). First, the code allows for two separate regions, an upper one with fine grid spacing, and a lower one with three-times the grid spacing. This feature allows for a fine grid space near the surface where shear-wave velocities are low without carrying the fine spacing to depth where it is not needed. In addition, the grid spacing can be made to grow in the horizontal and vertical directions, giving a further savings in computational effort. In this code we also improve the modeling of attenuation. The code has been fully tested and validated.

A preliminary investigation on the developed algorithms was performed using the synthetic data generated from a simple 3D velocity structure (Figure 1). We have tested the effects of initial velocity model on the inversion results. We also tested different formula for updating the Hessian matrix.

2. Formulation of the inversion problem

In this section, we define the inverse problem in terms of an objective function and derive the expression for the Frechet derivative of the objective function.

The velocity structure model parameters $c(\mathbf{x})$ (P-wave velocity, $\alpha(\mathbf{x})$, or S-wave velocity, $\beta(\mathbf{x})$) are determined from the inversion of recorded seismograms by minimizing the following objective function:

$$E(\mathbf{M}) = \frac{1}{2}\left\{ W_T \sum_s \sum_r \sum_m (\Delta T_m^{rs})^2 + W_W \sum_s \sum_r \sum_m [W_m^{rs} \int \Delta u_m^2(\mathbf{x}_r, t; \mathbf{x}_s) dt] \right\} \tag{1}$$

where,

$$\Delta u_m(\mathbf{x}_r, t; \mathbf{x}_s) = u_m(\mathbf{x}_r, t; \mathbf{x}_s) - o_m(\mathbf{x}_r, t; \mathbf{x}_s),$$
$$W_m^{rs} = 1 \Big/ \int [o_m(\mathbf{x}_r, t; \mathbf{x}_s)]^2 dt,$$

and $\mathbf{M}$ is the vector of velocity model parameters; $u_m(\mathbf{x}_r, t; \mathbf{x}_s)$ is the mth component of synthetic displacement at receiver $\mathbf{x}_r$ generated by a seismic source at $\mathbf{x}_s$; $o_m(\mathbf{x}_r, t; \mathbf{x}_s)$ is the corresponding observed displacement; and $\Delta T_m^{rs} = T_m^{\mathrm{cal}}(\mathbf{x}_r, \mathbf{x}_s) - T_m^{\mathrm{syn}}(\mathbf{x}_r, \mathbf{x}_s)$ is the difference between the observed and calculated first arrival time; W_T and W_W are used to adjust the weight of the contribution to the objective function from the fitting of the travel-times and waveforms.

In practice, seismic travel-times can be found either by hand-picking the first arrival time or by some automated method. However, picked times corresponds to the arrival of the highest-frequency observable waves. The widespread availability of broad-band digital data has led to the recent development of automated travel-time measurement techniques, based upon the cross-correlation of observed body wave phases with the corresponding synthetics (e.g., Luo and Schuster, 1991; Marquering *et al*. 1999). First we define the cross-correlation of the synthetic and observed waveform as

$$f(\Delta T) = W_m^{rs} \int [u_m(\mathbf{x}_r, t; \mathbf{x}_s) o_m(\mathbf{x}_r, t + \Delta T; \mathbf{x}_s)] dt\,. \tag{2}$$

Then the travel-time difference ΔT_m^{rs} is directly determined by finding the maximum of Equation (2), that is

$$f(\Delta T_m^{rs}) = \max\{ f(\Delta T) \,|\, \Delta T \in [-\Delta T_{\max}, \Delta T_{\max}] \}\,. \tag{3}$$

Here $\Delta T_{\max}$ is the estimated maximum travel-time difference between the observed and synthetic seismograms.

Because synthetic seismograms are nonlinearly related to the velocity of the earth structure, the objective function defined in equation (1) contains many local minima. While a global optimization method, such as simulated annealing or genetic algorithm (e.g., Sen and Stoffa 1995), may seem to be a good technique to minimize this objective function, it is impractical to perform this kind of inversion at present because the global method needs to evaluate the objective function for many different model parameters. As an alternative, a generalized gradient method, such as steepest descent or quasi-Newton (e.g., Fletcher, 1987; Tarantola, 1987), is often used to invert for velocity structure. The disadvantage of gradient methods is that they are likely to converge to one of the local minima instead of the global minimum. However they have the advantage of being very efficient.

Regardless of which kind of gradient method is used, it always requires at least the first order derivative of the objective function with respect to the model structure parameters, which is given by

$$\frac{\partial E}{\partial c} = W_T \sum_s \sum_r \sum_m (\Delta T_m^{rs}) \frac{\partial \Delta T_m^{rs}}{\partial c} + W_W \sum_s \sum_r \sum_m W_m^{rs} \int \Delta u_m(\mathbf{x}_r, t; \mathbf{x}_s) \frac{\partial u_m(\mathbf{x}_r, t; \mathbf{x}_s)}{\partial c} dt \,, \tag{4}$$

where $\partial \Delta T/\partial c$ and $\partial u/\partial c$ are the Frechet derivative of travel-time difference and displacement, respectively. Luo and Schuster (1991) present an explicit expression for the Frechet derivative of a seismic travel-time measured by the cross-correlation of an observed and a synthetic waveform. This Frechet derivative is of the form

$$\frac{\partial \Delta T_m^{rs}}{\partial c(\mathbf{x})} = D_m^{rs} \int [\dot{o}_m(\mathbf{x}_r, t + \Delta T_m^{rs}; \mathbf{x}_s) \frac{\partial u_m(\mathbf{x}_r, t; \mathbf{x}_s)}{\partial c}] dt \tag{5}$$

where

$$D_m^{rs} = 1 \Big/ \int [\dot{o}_m(\mathbf{x}_r, t + \Delta T_m^{rs}; \mathbf{x}_s) \dot{u}_m(\mathbf{x}_r, t; \mathbf{x}_s)] dt \,.$$

Marquering *et al*. (1999) independently derived an equivalent form of the Frechet derivative of travel-time difference. From equation (5) we find that the Frechet derivative of travel-time difference is calculated from the Frechet derivative of displacement. Substitution of equation (5) into equation (4) gives

$$\frac{\partial E}{\partial c} = \sum_s \sum_m \left\{ \sum_r \int [W_T D_m^{rs} \Delta T_m^{rs} \dot{o}_m(\mathbf{x}_r, t + \Delta T_m^{rs}; \mathbf{x}_s) + W_W W_m^{rs} \Delta u_m(\mathbf{x}_r, t; \mathbf{x}_s)] \frac{\partial u_m(\mathbf{x}_r, t; \mathbf{x}_s)}{\partial c} dt \right\} \tag{6}$$

In the following we derive the expression for the Frechet derivative of synthetic displacement. Let $\mathbf{u}(\mathbf{x}, t; \mathbf{x}_s)$ be the three-component displacement response of the elastic earth model at location $\mathbf{x}$ to a body force $\mathbf{F}$ applied at time t=0 at a source point $\mathbf{x}_s$, then the response can be described by the wave equation

$$\rho \ddot{u}_m - \partial_m(\lambda \partial_i u_i) - \partial_i[\mu(\partial_i u_m + \partial_m u_i)] = F_m \qquad m=1, 2, 3, \text{ and } t \in [0, T], \tag{7}$$

subject to the free surface boundary condition and the initial conditions

$$u_m(\mathbf{x}, 0; \mathbf{x}_s) = 0 \text{ , and } \dot{u}_m(\mathbf{x}, 0; \mathbf{x}_s) = 0$$

where

$$\ddot{u}_m = \frac{\partial^2 u_m}{\partial t^2}, \; \dot{u}_m = \frac{\partial u_m}{\partial t}, \text{ and } \partial_i = \frac{\partial}{\partial x_i};$$

and the summation convention for repeated subscripts is assumed (e.g. $\partial_i u_i = \partial_1 u_1 + \partial_2 u_2 + \partial_3 u_3$); ρ, λ, and μ are the density and Lame parameters of the earth model, respectively. If $\mathbf{F}$ is the equivalent body force of the seismic moment tensor, then $\mathbf{u}$ is the displacement wave generated from a seismic point source. If $\mathbf{F}$ is a unit impulse applied in the *n*th direction, the displacement u_m is denoted as the Green's function $g_m^n(\mathbf{x}, t; \mathbf{x}_s)$.

According to the Born approximation, a small perturbation in Lame parameters of the earth model parameters,

$$\lambda(\mathbf{x}) \to \lambda(\mathbf{x}) + \delta\lambda(\mathbf{x}), \qquad \mu(\mathbf{x}) \to \mu(\mathbf{x}) + \delta\mu(\mathbf{x}),$$

will produce a wave field

$$u_m(\mathbf{x}, t; \mathbf{x}_s) \to u_m(\mathbf{x}, t; \mathbf{x}_s) + \delta u_m(\mathbf{x}, t; \mathbf{x}_s).$$

If we assume that the Lame parameters are subject to a perturbation in the volume Ω, the corresponding perturbation of displacement $\delta u_m(\mathbf{x}_r, t; \mathbf{x}_s)$ can be represented (e.g. Marquering *et al*, 1999; Zhao *et al*, 2002) as

$$\begin{aligned}\delta u_m(\mathbf{x}_r, t; \mathbf{x}_s) = &-\int_\Omega \delta\alpha 2\rho\alpha[\partial_i u_i(\mathbf{x}, t; \mathbf{x}_s)] * [\partial_k g_k^m(\mathbf{x}, t; \mathbf{x}_r)] d\Omega \\ &+ \int_\Omega \delta\beta 4\rho\beta[\partial_i u_i(\mathbf{x}, t; \mathbf{x}_s)] * [\partial_k g_k^m(\mathbf{x}, t; \mathbf{x}_r)] d\Omega \\ &- \int_\Omega \delta\beta 2\rho\beta[\partial_i u_k(\mathbf{x}, t; \mathbf{x}_s) + \partial_k u_i(\mathbf{x}, t; \mathbf{x}_s)] * [\partial_i g_k^m(\mathbf{x}, t; \mathbf{x}_r)] d\Omega\end{aligned} \tag{8}$$

where symbol * denote the temporal convolution. Implicit in the above relationship is that the density distribution is known. We make this assumption because (1) seismic travel-time is insensitivity to density; (2) the fewer the number of free parameters, the more stable the velocity inversion will be; and (3) empirical relations between velocity and density are available.

We know that equation

$$\delta u_m(\mathbf{x}_r, t; \mathbf{x}_s) = \frac{\partial u_m(\mathbf{x}_r, t; \mathbf{x}_s)}{\partial \alpha}\delta\alpha + \frac{\partial u_m(\mathbf{x}_r, t; \mathbf{x}_s)}{\partial \beta}\delta\beta \tag{9}$$

is defined for any δα and δβ. From this equation and equation (8) we can obtain the derivative of displacement used in equation (6). However, in most cases we will not explicitly compute the Green's function $g_k^m(\mathbf{x}, t; \mathbf{x}_r)$ used in equation (8) (Tarantola, 1987). Instead, similar to the study of Tromp *et al*. (2005), we introduce the back-propagation wavefield $\Psi(\mathbf{x}, t; \mathbf{x}_s)$ defined as

$$\psi_k(\mathbf{x}, t; x_s) = \int g_k^m(\mathbf{x}, t' - t; x_r)[W_T D_m^{rs} \Delta T_m^{rs} \dot{o}_m(\mathbf{x}_r, t' + \Delta T_m^{rs}; \mathbf{x}_s) + W_W W_m^{rs} \Delta u_m(\mathbf{x}_r, t'; \mathbf{x}_s)] dt'. \tag{10}$$

Based on equations (6), (8) and (10), the variation of the objective function due to a perturbation δα(**x**) and δβ(**x**) can be represented as

$$\begin{aligned}\delta E[\mathbf{M}(\mathbf{x})] = \sum_s \int dt \{ &-2\rho\alpha[\partial_i u_i(\mathbf{x}, t; \mathbf{x}_s)][\partial_k \psi_k(\mathbf{x}, t; \mathbf{x}_s)]\delta\alpha \\ &+ 4\rho\beta[\partial_i u_i(\mathbf{x}, t; \mathbf{x}_s)][\partial_k \psi_k(\mathbf{x}, t; \mathbf{x}_r)]\delta\beta \\ &- 2\rho\beta[\partial_i u_k(\mathbf{x}, t; \mathbf{x}_s) + \partial_k u_i(\mathbf{x}, t; \mathbf{x}_s)][\partial_i \psi_k(\mathbf{x}, t; \mathbf{x}_r)]\delta\beta \}\end{aligned} \tag{11}$$

For the convenience of computing the Frechet derivatives with a staggered-grid finite difference scheme, we reorganize the above equation and finally get the derivatives of the objective function as

$$\begin{aligned}\frac{\partial E[\mathbf{M}(\mathbf{x})]}{\partial \alpha(\mathbf{x})} &= \sum_s \int dt \left\{ -\frac{2\alpha}{\rho(3\alpha^2 - 4\beta^2)^2}[\tau_{ii}(\mathbf{x}, t; \mathbf{x}_s)][\sigma_{kk}^m(\mathbf{x}, t; \mathbf{x}_s)] \right\} \\ \frac{\partial E[\mathbf{M}(\mathbf{x})]}{\partial \beta(\mathbf{x})} &= \sum_s \int dt \left\{ \frac{3\alpha^4 - 7\alpha^2\beta^2 + 6\beta^4}{\rho(3\alpha^2 - 4\beta^2)^2\beta^3}[\tau_{ii}(\mathbf{x}, t; \mathbf{x}_s)][\sigma_{kk}(\mathbf{x}, t; \mathbf{x}_s)] \right. \\ &\qquad \left. - \frac{1}{\rho\beta^3}[\tau_{ik}(\mathbf{x}, t; \mathbf{x}_s)\sigma_{ki}(\mathbf{x}, t; \mathbf{x}_s) \right\}\end{aligned} \tag{12}$$

where τ and σ are the stresses,

$$\begin{aligned}\tau_{ij}(\mathbf{x}, t; \mathbf{x}_s) &= \lambda\partial_k u_k(\mathbf{x}, t; \mathbf{x}_s)\delta_{ij} + \mu(\partial_i u_j(\mathbf{x}, t; \mathbf{x}_s) + \partial_j u_i(\mathbf{x}, t; \mathbf{x}_s) \\ \sigma_{ij}(\mathbf{x}, t; \mathbf{x}_s) &= \lambda\partial_k \psi_k(\mathbf{x}, t, ; \mathbf{x}_s)\delta_{ij} + \mu(\partial_i \psi_j(\mathbf{x}, t; \mathbf{x}_s) + \partial_j \psi_i(\mathbf{x}, t; \mathbf{x}_s)\end{aligned}, \tag{13}$$

In the following section we will present a procedure to calculate these stresses, as well as the displacements and velocities at recording stations from seismic sources.

3. Calculations of Synthetic Wave Fields

The three-dimension seismic wave propagation problem is currently solved by discrete numerical methods such as finite-difference, finite-element, spectral-element, and pseudospectral methods. In general there are two ways to apply these methods to calculate the 3D synthetic seismograms or Green's functions. First, applying forces at a point source, the seismograms can be obtained at various receivers. Second, using reciprocity relationship of Green's functions, body forces are applied at a receiver location and the seismograms can be calculated for all sources. Liu and Archuleta (1999a, 2003) have already applied reciprocity to calculate 3D Green's functions using the finite difference method for their inversion of the rupture process of large earthquakes.

To solve the inverse problem defined in this report, we need to compute the three-component seismic displacements and velocities at all recording stations, and stresses at all the locations where material velocities will be perturbed. Let us assume that there are *NP* point sources and *NR* receivers in our study. Based on the above discussion, if 2•*NP* is greater than 3•*NR*, we will calculate the Green's functions by applying an impulse body force separately for each component of each receiver. This reciprocity requires 3•*NR* computations to obtain all the Green's functions. If not, for each earthquake we will first perform one straightforward computation to get all the synthetic seismograms, and then compute the back-propagation wavefield $\Psi(\mathbf{x},t;\mathbf{x}_s)$ generated from the weighted residuals at all receivers. In this case, the total computations will be 2•*NP*, regardless of the number of receivers. As indicated by Tarantola (1987), the wavefield $\Psi(\mathbf{x},t;\mathbf{x}_s)$ is the solution of the following wave equation,

$$\rho\ddot{\psi}_m - \partial_m(\lambda\partial_i\psi_i) - \partial_i[\mu(\partial_i\psi_m + \partial_m\psi_i)] = \phi_m(\mathbf{x},t;\mathbf{x}_s), \quad m=1, 2, 3, \text{ and } t \in [0, T], \tag{14}$$

subject to the free surface boundary condition and the final (instead of initial) conditions

$$\psi_m(\mathbf{x},T;\mathbf{x}_s)=0 \text{ , and } \dot{\psi}_m(\mathbf{x},T;\mathbf{x}_s)=0,$$

where,

$$\phi_m(\mathbf{x},t,\mathbf{x}_s) = \sum_r \delta(\mathbf{x}-\mathbf{x}_r)[W_T D_m^{rs}\Delta T_m^{rs}\dot{o}_m(\mathbf{x}_r, t+\Delta T_m^{rs};\mathbf{x}_s) + W_W W_m^{rs}\Delta u_m(\mathbf{x}_r,t;\mathbf{x}_s)]. \tag{15}$$

We will use a 3D viscoelastic finite difference (FD) algorithm of Liu and Archuleta (2002) for these numerical computations. The FD algorithm is accurate to fourth order in space and second order in time. It employs the staggered-grid, velocity-stress formulation. Therefore we can directly obtain the velocities and stresses from the FD computation. The displacements are calculated through integration of the corresponding velocities. This code includes coarse-grained attenuation (Liu and Archuleta, 1999b). It can simulate frequency-dependent or constant *Q* in the time domain. Another desirable feature of the code is that it implements a grid with variable spacing. Basically, the grid system is divided into two regions: Region **I** is the volume that includes the free surface, and Region **II** is all the volume below the Region **I**. The grid spacing in the horizontal direction is three times coarser in Region **II** compared to Region **I**. A general observation is that the material velocity near the free surface is generally small relative to most of the volume and can strongly affect the ground motion. This low-velocity material will impose the most severe computational and memory requirements. The FD algorithm with variable-grid spacing is one approach to efficiently incorporate the low-velocity layer into FD

simulation. Compared to a FD algorithm with regular grid spacing, the FD algorithm with variable-grid spacing requires one-quarter the memory and one-fifth the CPU time. This feature is fundamental to the velocity structure inversion because of the large amount of computations required to calculate the synthetics.

To efficiently incorporate the effects of Q into our 3D FD numerical simulations of wave propagation, we derive an empirical formula for modeling an arbitrary Q that can be a function of frequency (Liu and Archuleta, 2006). Another key issue in the implementation of variable-grid spacing is how to interpolate the wave field on the interface of Region **I** and Region **II**. Almost all variable-grid FD algorithms use linear interpolation because it does not lead to an unstable problem, but the accuracy of the simulation is not ideal. Through a large number of numerical tests we have found an improved interpolation scheme that is both accurate and stable.

4. Inversion Method

The inverse problem in this report is defined as finding the nonlinear least square (L_2 norm) solution. It has the following characteristics

(1) the objective function $E(\mathbf{M})$ is nonlinear;
(2) the evaluations of $E(\mathbf{M})$ and its Frechet derivatives are very expensive.
(3) the number of free parameters **M** to be inverted for may be several thousand.

While a global inversion method, such as simulated annealing or genetic algorithm (Sen and Stoffa 1995), is desirable to solve a nonlinear problem, the requirement of solving a large number (on the order of millions) of forward problems prohibits the application of global methods to our inverse problem. In practice, a local inversion method based on the gradient of the objective function is used to invert for 2D or 3D velocity structure (Tarantola, 1987), although it is well known that this kind of method may find a local minima rather than a global minimum.

There is a wide range of local inversion methods that can be chosen to iteratively solve our nonlinear least square problem. It is best to consider the above characteristics of our problem in making a decision. It is most difficulty to address the characteristic (1) with a local method because a good initial velocity model is necessary. We will adopt a multiscale waveform inversion strategy (Bunks, *et al*., 1995) to reduce the dependence of the final solution on the initial model. In addition, we plan to choose a non-monotone trust-region algorithm which is based on Quasi-Newton method, because it has better global convergence properties, comparing to Cauchy methods such as steepest descent. The characteristic (2) is another serious impediment to solving our inverse problem. It limits the number of iterations that can be performed, thus requiring that the method have a rapid rate of convergence. The characteristic (3) means that the size of this problem is moderate. This feature allows us to have certain flexibility in selecting a local method without too much concern for RAM and CPU time required by the method itself.

Both Newton-like (quasi-Newton, strictly speaking) and Cauchy methods are widely used for solving nonlinear geophysics problems (e.g., Tarantola, 1987; Hartzell, 1989). However quasi-Newton methods are recognized today as one of the most efficient ways to solve nonlinear unconstrained or bounded constrained optimization problems. These methods are mostly used when the second derivative matrix (Hessian matrix) of the objective function is either unavailable or too costly to compute. They are like Newton's method except that the Hessian matrix is approximated by a symmetric matrix, which is corrected or updated from iteration to iteration.

Quasi-Newton methods can be divided into two categories: one kind using a "line search" algorithm, another using a "trust region" algorithm. To implement the line search" algorithm, requires maintaining a positive definite approximation to the Hessian matrix of the objective function, such that the line search follows a descent direction in the objective function. Otherwise the algorithm loses its search direction. Although the true Hessian is usually positive definite at the solution of the problem, this may not be the case when the current iteration of the algorithm is far from convergence. As an alternative, the trust region algorithm is a more effective approach to circumventing the difficulty caused by a non-positive definite Hessian matrix. As pointed out by Fletcher (1987), a particular advantage of trust region algorithms is that they retain the rapid rate of convergence of Newton's method, but are generally applicable and globally convergent, with no significant restriction on the class of problem to which they apply.

Based on the above discussion, we selected a quasi-Newton trust region algorithm. In the rest of this section, we first describe the trust region algorithm and its implementation, and then find a way to approximate the Hessian matrix.

There are several versions of trust-region methods that can be chosen. Our description of the trust-region method mostly follows Conn, *et al*. (2000), except that we use a global optimization method to minimize the quadratic model of the objective function. Starting from an initial model $\mathbf{M}^0$, the trust-region algorithm iteratively looks for the best solution. At each iterate $\mathbf{M}^k$, the algorithm first assumes that the objective function $E(\mathbf{M}^k)$ can be approximated by its quadratic model $q(\delta\mathbf{M})$ within a suitable neighborhood Δ^k of $\mathbf{M}^k$, which is referred to as the trust region. The $q(\delta\mathbf{M})$ has the form

$$E(\mathbf{M}^k + \delta\mathbf{M}) \approx q^k(\delta\mathbf{M}) = E(\mathbf{M}^k) + \mathbf{A}^{\mathrm{T}}\delta\mathbf{M} + \delta\mathbf{M}^{\mathrm{T}}\mathbf{B}^k\delta\mathbf{M} \tag{15}$$

where $\delta\mathbf{M} = \mathbf{M} - \mathbf{M}^k$; vector $\mathbf{A}^k$ indicates the first-order gradient of the objective function $E(\mathbf{M}^k)$; symmetric $\mathbf{B}^k$ is an approximation to the Hessian matrix (second-order derivative) of $E(\mathbf{M}^k)$ as discussed later.

Then a trial model $\bar{\mathbf{M}}^{k+1} = \mathbf{M} + \delta\mathbf{M}^k$ is constructed by finding the solution $\delta\mathbf{M}^k$ of the following subproblem:

$$\text{Minimize}\left\{q^k\left(\delta\mathbf{M}\right)\right\} \quad \text{subject to } \|\delta\mathbf{M}\|_\infty \le \Delta^k \tag{16}$$

where $\|\bullet\|_\infty$ denotes the infinity norm. The acceptance of the trial model and the modification of Δ^k depend on the ratio η^k of the actual reduction in the objective function to the predicted reduction of the quadratic model. To achieve a better global convergence, we use a ratio η^k that is defined by not only comparing the actual versus predicted reduction during the current iteration but also capturing the trend over some past history. It has the form

$$\eta^k = \max[\eta_h^k, \eta_c^k], \tag{17}$$

where

$$\eta_h^k = [E(\mathbf{M}^{r(k)}) - E(\mathbf{M}^k + \delta\mathbf{M}^k)]/[E(\mathbf{M}^{r(k)}) - q^k(\delta\mathbf{M}^k)],$$
$$\eta_c^k = [E(\mathbf{M}^k) - E(\mathbf{M}^k + \delta\mathbf{M}^k)]/[E(\mathbf{M}^k) - q^k(\delta\mathbf{M}^k)],$$

and the index $r(k)$ denotes a reference iteration in history with $r(k) \le k$ and $r(0) = 0$. Conn et al (2000) describe a way in detail to determine the $r(k)$. Based on this accepting criterion the objective function no longer reduces monotonically during the iteration process.

Finally the iterate $\mathbf{M}^k$ is updated by setting

$$\mathbf{M}^{k+1} = \begin{cases} \mathbf{M}^k + \delta\mathbf{M}^k & \text{if } \eta^k > 0.05 \\ \mathbf{M}^k & \text{if } \eta^k \le 0.05 \end{cases}. \tag{18}$$

The trust region bound Δ^k is updated by setting

$$\Delta^{k+1} = \begin{cases} 0.5\,\|\,\delta\mathbf{M}^k\|_\infty & \text{if } \eta^k \le 0.05 \\ \Delta^k & \text{if } 0.05 < \eta^k < 0.9 \\ \max[2.5\,\|\,\delta\mathbf{M}^k\|_\infty, \Delta^k] & \text{if } \eta^k \ge 0.9 \end{cases}. \tag{19}$$

In order to induce a fast asymptotic rate of convergence of the trust region method, we normally require a good approximation to the minimizer of (16). However in certain cases it may not be easy to find the global solution of (16) because of the box constraint and the possibility that **B** can have negative eigenvalues (Conn, et al, 1991). Several methods have been proposed to solve equation (16) (see Fletcher, 1987; and Conn et al., 1988). Of them the Levenberg-Marquardt type methods are the most well known. However all these methods are designed to find an approximate solution of this equation (of course, when the matrix **B** is positive definite, the solution is global).

Here we use a particular kind of the simulated annealing method, called the heat-bath algorithm (Rothman 1986), to find the global solution of (16). This algorithm, as point out by Sen and Stoffa (1995), is good for problems with a large number of free parameters. It is not efficient to solve quadratic problems using a global method. Compared to the local methods mentioned above, it requires much more computing time. However this computing time is negligible compared with the time required to compute the synthetic seismograms and the Frechet derivatives of the objective function. Given the fact that a global solution of (16) is very important for the trust region method to achieve a fast rate of convergence, we believe it is worth adopting a global method in our inverse problem. We use a global optimization method only for solving equation (16) rather than for minimizing the objective function of the inverse problem.

Besides solving equation (16), the other major consideration in implementing the trust-region algorithm is the choice of the method to determine the matrix $\mathbf{B}^k$. Because the Hessian matrix of the objective function is too costly to compute in practice, the matrix $\mathbf{B}^k$ is often calculated by using a quasi-Newton technique, such as B.F.G.S. method or symmetric rank-one method (Fletcher, 1987). The B.F.G.S. method updates the $\mathbf{B}^k$ using the following formula

$$\mathbf{B}^k = \mathbf{B}^{k-1} + \frac{\mathbf{B}^{k-1}\delta\mathbf{M}^{k-1}(\delta\mathbf{M}^{k-1})^{\mathrm{T}}\mathbf{B}^{k-1}}{(\delta\mathbf{M}^{k-1})^{\mathrm{T}}\mathbf{B}^{k-1}\delta\mathbf{M}^{k-1}} + \frac{(\mathbf{A}^k - \mathbf{A}^{k-1})(\mathbf{A}^k - \mathbf{A}^{k-1})^{\mathrm{T}}}{(\mathbf{A}^k - \mathbf{A}^{k-1})^{\mathrm{T}}\delta\mathbf{M}^{k-1}}, \tag{20}$$

and the symmetric rank one (SR1) formula is of the form

$$\mathbf{B}^k = \mathbf{B}^{k-1} + \frac{[(\mathbf{A}^k - \mathbf{A}^{k-1}) - \mathbf{B}^{k-1}\delta\mathbf{M}^{k-1}][(\mathbf{A}^k - \mathbf{A}^{k-1}) - \mathbf{B}^{k-1}\delta\mathbf{M}^{k-1}]^{\mathrm{T}}}{[(\mathbf{A}^k - \mathbf{A}^{k-1}) - \mathbf{B}^{k-1}\delta\mathbf{M}^{k-1}]^{\mathrm{T}}\delta\mathbf{M}^{k-1}}. \tag{21}$$

We will test both formulas for updating the Hessian matrix during the inversion of velocity structure.

5. Example

To evaluate the inversion procedure presented in previous sections, we apply it to determine a simple 3D velocity structure using synthetic seismograms. The target 3D velocity model is shown in Figure 1. The model has a half-ellipsoid basin within the half space. The size

and the shape of the model are labeled in the plots of Figure 1. We assumed that two small scenario earthquakes are recorded by a dense array (Figure 2) deployed within the studied area. The locations of the two earthquakes are shown in the Figures 2. Their source parameters are given in Table 1. The slip rate of sources has the shape of Brune's source function:

$$\dot{s}(t) = \left(\frac{2\pi}{\tau}\right)^2 \exp\left(-\frac{2\pi t}{\tau}\right). \tag{22}$$

In which, the τ denotes the slip rise-time.

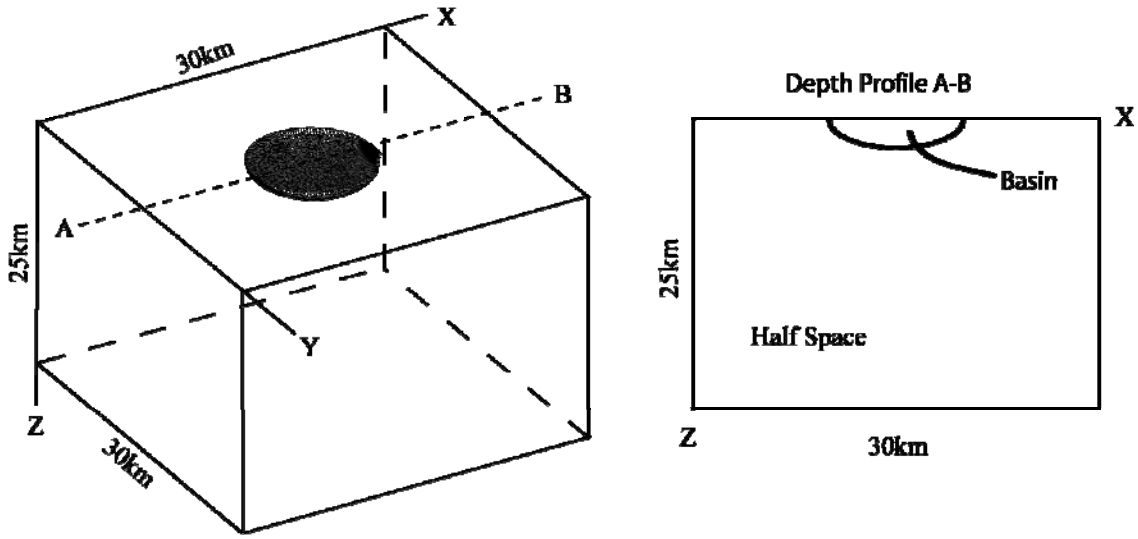

Figure 1. The 3D velocity structure model and the Finite Difference simulation range.

When quasi-Newton trust region algorithm is applied to minimize the objective function defined in equation (1), we need to compute the Frechet derivatives for the objective function. Using the back-propagation wave field and equation (12) is the most efficient way to obtain the Frechet derivatives. However, as pointed out by Tromp et al. (2005), we need to have simultaneous access to the regular wave field and the back-propagation wave field, and to low-pass filter both wave fields to remove the dispersion influence of FD simulation. Therefore both wave filed need to be stored as function of space and time. At present the Linux cluster used for this study does not have enough hard disk memory to store these wave fields. As an alternative we directly apply the equation (6) to calculate Frechet derivatives. The derivatives of synthetic ground motion versus the parameters of structure model are approximated by the difference:

$$\frac{\partial u_m(c,t)}{\partial c} \approx \frac{u_m(c+\Delta c,t) - u_m(c,t)}{\Delta c}, \tag{23}$$

where, we set $\Delta c = 0.02c$.

In this test we invert for the P-wave and S-wave velocities of the basin and half space using waveform data. The densities will not change during the inversion and are set the same as the target model. But the *Q* values are a function of S-wave velocity. We use same relationship between *Q* and S-wave velocities to compute the synthetic data and to calculate the regular and the back-propagation wave field. As shown in figure 2, thirty-six three-component ground velocities are used in the inversion. Both 'data' and simulations are low-pass filtered with corner frequency of 1.0 Hz. The initial inversion values of P-wave and S-wave velocities are listed in Table 2. They are about 15 percent away from the target values. In the same table we also list the

bound of each free parameter used in the inversion procedure. We set the initial trust region with value of 0.1. This means that a parameter can be perturb about 10 percent of its value.

Table 1. Earthquake locations and their source parameters

Event #	X (m)	Y (m)	Depth (m)	Moment (N-m)	Rise Time (sec)	Strike (°)	Dip (°)	Rake (°)
1	8000	8000	10000	$1.0*10^{12}$	0.3	120	60	70
2	20000	20000	7000	$5.0*10^{11}$	0.2	340	70	20

Table 2. Target and Initial Velocity Structure Models

Model	Basin P-velocity (m/s)	Basin S-velocity (m/s)	Basin Density (kg/m^3)	Half Space P-velocity (m/s)	Half Space S-velocity (m/s)	Half Space Density (kg/m^3)
Target	2000	1000	2100	5400	3100	2700
Initial	2300	1200	2100	5900	3500	2700
Bounds	1600-2400	600-1500		5000-6000	2500-3700	

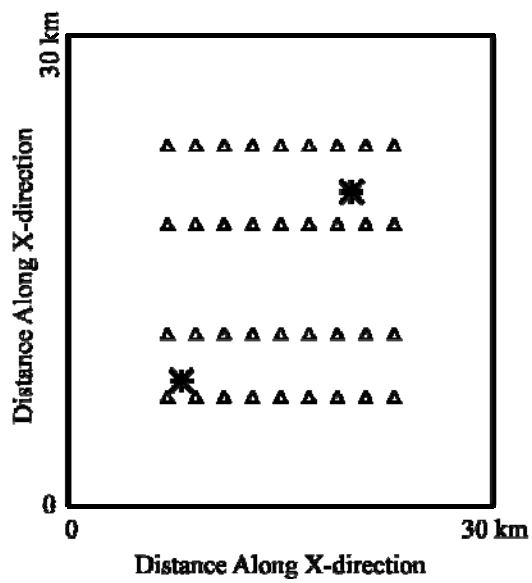

Figure 2. Map of recording stations (triangles) used in the inversion for velocity structure. The stars denote two earthquake epicenters.

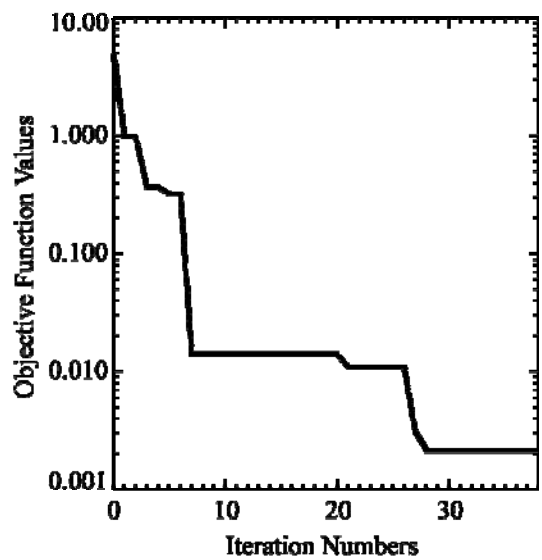

Figure 3. The objective function values versus the number of iterations

Figure 3 plots the misfit between the 'data' and synthetics as the function of iteration number. From Figure 3 we can see that the inversion converges to the target model after 28 iterations. The objective function has a value of 0.15 at the iteration 8. The inverted result from this iteration matches the target model with an error of less than 1%. However this result is not a global but a local minimum solution. The inversion process then takes about 20 steps more to search the model space and escape from local minima. This means the algorithm exhausts most of the computing time to move from a very good model to the best (true) model. This feature can

results from the error in the estimating of Hessian matrix and/or from the error of difference calculation in term of equation (23).

This test indicated that, if the initial model is not far away from the true model, the quasi-Newton trust region algorithm can efficiently solve the waveform inversion problem. To test the influence of initial model, we ran another inversion using half space as initial model, i.e. the initial values P-wave and S-wave velocities are set same for the basin and half space, respectively. In this test the inversion process only run 5 iterations and then stoped. The output is far away from the true model. The reason may be (1) the dependence of the inversion algorithm on the initial model; and/or (2) large error in the calculation of Frechet derivatives when equation (23) is implemented. We have done a test using $\Delta c = 0.01c$ and $\Delta c = -0.01c$, respectively. We find that the values of Frechet derivatives can have different sign when using different values of Δc.

During the inversion, we separately used the B.F.G.S formula (Eq. 20) and SR1 formula (Eq. 21) to update the Hessian matrix. Although Conn *et al*. (1991) point out that the SR1 updating normally performs better than B.F.G.S. when combined with a trust-region algorithm, our testing show that B.F.G.S. updating performs better than the SR1 updating for the inversion of waveform data.

6. Discussion and Conclusion

We develop a method and procedure to determine 3D velocity structure from the inversion of waveform data. This procedure needs to compute the regular wave field and back-propagation wave field for each earthquake. Both wave fields are calculated using a finite difference method. The objective function of the inversion consists of a weighted sum of the difference between the observed and synthetic first arrival times and the sum of the squared differences of the waveforms. By using this objective function we can easily move from a purely travel-time based measure to a full waveform-based measure. We apply a non-monotone trust-region algorithm to solve the nonlinear inversion problem, which has better global convergence properties.

To limit computer requirements, we used a simple 3D velocity structure model to evaluate the performance of the presented procedure. This testing indicates that the quasi-Newton trust region algorithm converges very fast if the initial model relatively close to (~15% difference) the true model. Although the test problem is simple, it proves that the inversion algorithm can escape, at least, from shallow local minima, and move the trial model to the true solution. This testing also shows that B.F.G.S updating of the Hessian matrix performs better than the SR1 updating for the inversion of waveform data

However the algorithm did not converge to the target model when the initial model is far away from the true solution. This failure may result from the large errors in the calculation of Frechet derivatives. More testing will be performed in the future studies using equation (12) to compute the Frechet derivatives. This test will help to identify it is the Frechet derive calculation or the inversion method itself that cause the lacks of convergence. Also we will try other initial models to continually test the dependence of inversion algorithm on the starting model.

It is complex problem to determine 3D velocity structure from the inversion of seismic waveform data. More effort is required to improve and test the presented method. The implementation of the non-monotone trust region algorithm requires the specification of several free parameters. The optimum choice of these free parameters can improve the efficiency of the algorithm but is problem dependent. The values of these parameters used in our testing come

from the suggestions of Conn et al (2000). We will perform more velocity inversions using small models and synthetic data to find optimal values for the 3D velocity inversion problem. In future work we will consider determining the basin shape, as well as the values P-wave and S-wave velocity, from the inversion of waveforms.

7. Reference

Aoi, Shin (2002). Boundary shape waveform inversion for estimating the depth of three-dimensional basin structure, *Bull. Seism. Soc. Am.* **92**, 2410-2418.

Conn, A.R., N.I.M. Gould, and Ph.L. Toint (2000). *Trust-Region Methods*, MPS/SIAM Series on Optimization 1, SIAM, Philadelphia.

Conn, A., N. Gould, and P. Toint (1991). Convergence of quasi-Newton matrices generated by the symmetric rank one update, *Mathematical programming*, *50*, 177-196.

Conn, A., N. Gould, and P. Toint (1988). Testing a Class of Methods for solving minimization problems with simple bounds on the variables, *Mathematics of Computation*, **50**, 399-430.

Fletcher, R. (1987). *Practical methods of optimization*, John Wiley &Sons.

Graves, R. W., A. Pitarka, and P. G. Somerville (1998). Ground-motion amplification in the Santa Monica area: effects of shallow basin-edge structure, *Bull. Seism. Soc. Am.* **88**, 1224-1242.

Hartzell, S. H. (1989). Comparison of seismic waveform inversion results for the rupture history of a finite fault: application to the 1986 North Palm Springs, California, earthquake., *J. Geophys. Res*. **94**, 7515-7534.

Hartzell, S., E. Cranswick, A. Frankel, D. Carver, and M. Meremonte (1997). Variability of site response in the Los Angeles urban area, *Bull. Seism. Soc. Am.* **87**, 1377-1400.

Iwata, T., K. Hatayama, H. Kawase, and K. Irikura (1996). Site amplification of ground motions during aftershocks of the 1995 Hyogo-ken Nanbu earthquake in severely damaged zone-Array observation of ground motions in Higashinada Ward, Kobe City, Japan, *J. Phys. Earth* **44**, 553-561.

Ji, C., D. V. Helmberger, and D. J. Wald (2000). Basin structure estimation by waveform modeling: Forward and inverse methods, *Bull. Seism. Soc. Am.* **90**, 964-976.

Kawase, H. (1996). The cause of the damage belt in Kobe: "The basin-edge effect", constructive interference of the direct S-wave with the basin-induced diffracted/Raleigh waves, *Seism. Res. Lett.* **67**, (5), 25-34.

Liu, P-C and R. Archuleta (2003). A new nonlinear finite fault inversion with 3D Green's functions: Application to 1989 Loma Prieta, California, earthquake. *J. Geophys. Res*.. **109**, B02318, doi:10.1029/2003JB002625, 2004

Liu, P-C. and R. Archuleta (2002). The effect of a low-velocity surface layer on the simulated ground motion. *Seism. Res. Lett*., 73, 267.

Liu, P-C and Arculeta, R. J. (1999a) Source parameter inversion using 3D Green's functions: Application to the 1996 Northridge, California earthquake 9abstruct), Eos Trans. AGU, **80**(46), Fall Meet. Suppl., F709.

Liu, P-C and R. Archuleta (1999b). Modeling of absorbing boundaries and Q for 3-D numerical computations, in *SCEC 1999 Annual Meeting Report*, September 29-30, Palm Springs, California, 75.

Liu, P-C and R. Archuleta (2006). Efficient modeling of *Q* for 3D numerical simulation of wave propagation, Bull. Seism. Soc. Am., **96**, in Press.

Luo, Y. and G. Schuster (1991). Wave-equation traveltime inversion, *Geophysics*, **56**, 645-653.

Marquering, H., F. Dahlen, and G. Nolet (1999). Three-dimensional sensitivity kernels for finite-frequency traveltimes: the banana-doughnut paradox, *Geophys. J. Int*., 137, 805-815.

Olsen, K. B. and R. J. Archuleta (1996). Three-dimensional simulation of earthquakes on the Los Angeles fault system, Bull. Seism. Soc. Am., 86, 575-596.

Pitarka, A., K. Irikura, T. Iwata, and T. Kagawa (1996). Basin structure effects in the Kobe area inferred from the modeling of ground motions from two aftershocks of the January 17, 1995 Hyogo-ken Nanbu earthquake, *J. Phys. Earth* **44**, 563-576.

Sen, M. and P. Stoffa (1995). *Global Optimization Methods in Geophysical Inversion*, Elsevier Science B. V., Amsterdam, The Netherlands.

Tarantola, A. (1987). *Inverse problem theory*, Elsevier Elsevier Science B. V., Amsterdam, The Netherlands.

Tromp, J. C. Tape, and Q. Liu (2005). Seismic tomography, adjoint methods, time reversals and banana-doughnut kernels, *Geopgys. J. Int*., **160**, 195-216.

Wald, D. J., and R. W. Graves (1998). The seismic response of the Los Angeles Basin, California, *Bull. Seism. Soc. Am.* **88**, 337-356.

Zhao, L., K. Olsen, and T. Jordan (2002). Efficient finite-difference calculation for the Frechet kernels in structural inversion, in the *Southern California Earthquake Center Annual Report*, pp.144.

REPORTS PUBLISHED

Liu, P-C and R. Archuleta (2006). Efficient modeling of *Q* for 3D numerical simulation of wave propagation, Bull. Seism. Soc. Am., **96**, doi: 10.1785/0120050173. (in Press)